Chiral effective-field theory in the $\Delta(1232)$ region. II. Radiative pion photoproduction

Vladimir Pascalutsa*

European Centre for Theoretical Studies in Nuclear Physics and Related Areas (ECT), Villa Tambosi, Villazzano, TN 38050, Italy*

Marc Vanderhaeghen†

Physics Department, The College of William & Mary, Williamsburg, Virginia 23187, USA and Theory Center, Jefferson Lab, 12000 Jefferson Avenue, Newport News, Virginia 23606, USA

(Received 1 October 2007; published 24 January 2008)

We present a theoretical study of the radiative pion photoproduction on the nucleon ($\gamma N \to \pi N \gamma'$) in the Δ-resonance region, with the aim to determine the magnetic dipole moment (MDM) of the $\Delta^+(1232)$. The study is done within the framework of chiral effective-field theory, where the expansion is performed (to next-to-leading order) in the δ power-counting scheme, an extension of chiral perturbation theory to the Δ-resonance energy region. We present the results for the absorptive part of the Δ MDM, as well as perform a sensitivity study of the dependence of $\gamma N \to \pi N \gamma'$ observables on the real part of the Δ MDM. We find that an asymmetry for circular polarization of the photon beam may provide a model-independent way to measure the Δ MDM.

DOI: 10.1103/PhysRevD.77.014027 PACS numbers: 12.39.Fe, 13.40.Em, 25.20.Dc

I. INTRODUCTION

The $\Delta(1232)$-isobar is the lowest nucleon excitation and the most distinguished baryon resonance. Unfortunately, its lifetime ($\approx 10^{-23}$ s) is far too short for a direct measurement of its electromagnetic moments. A measurement of the electromagnetic moments of such an unstable particle can apparently be done only indirectly, in a three-step process, where the particle is produced, emits a low-energy photon, which plays the role of an external magnetic field, and then decays. In this way the magnetic dipole moment (MDM) of Δ^{++} is accessed in the radiative pion-nucleon scattering ($\pi^+ p \to \pi^+ p \gamma$) [1], while the MDM of Δ^+ and Δ^0 can be accessed in the *radiative photoproduction* ($\gamma N \to \pi N \gamma'$) of neutral [2] and charged [3] pions, on the proton and neutron, respectively.

Some theoretical input is then needed in order to extract the MDM value from observables. For instance, the current Particle Data Group value of the Δ^+ MDM [4],

$$\mu_{\Delta^+} = 2.7^{+1.0}_{-1.3}(\text{stat}) \pm 1.5(\text{syst}) \pm 3(\text{theor})\mu_N, \qquad (1)$$

with $\mu_N = e/2M_N$ the nuclear magneton, was obtained by the TAPS Collaboration at MAMI [2] using a phenomenological model of the $\gamma p \to \pi^0 p \gamma'$ reaction [5]. The size of the error bar is rather large due to both experimental and theoretical uncertainties.

Recently a dedicated experimental effort took place at MAMI using the Crystal Ball detector [6], improving on the statistics of the TAPS data by almost 2 orders of magnitude. The present work is an effort to make an analogous improvement on the theoretical side by using a more consistent and systematic framework of chiral effective-field theory (χEFT). The first calculation within χEFT of the radiative pion photoproduction in the Δ-resonance region with the aim of extracting the Δ^+ MDM has been presented in [7]. In this more extended publication we present further details and make a few improvements on the first work.

The previous studies of the radiative pion photoproduction were based on the so-called "effective Lagrangian approach" [5,8,9], where one computes only the (unitarized) tree-level contributions, and "dynamical models" [10], where some pion rescattering effects are included in addition.

The framework of χEFT is more powerful in that it allows to compute the chiral-loop corrections in the consistent framework of quantum field theory (see, e.g., [11–14] for reviews). The chiral symmetry of the low-energy strong interaction, together with other general principles, such as unitarity and analyticity, is incorporated in χEFT to any given order in a systematic expansion over the energy scales and hadronic degrees of freedom.

In the problem at hand, the energy flow is defined by the energies of incoming and outgoing photon. To access the magnetic dipole moment of the Δ, the energy of the incoming photon must be sufficient to excite the resonance, while the emitted photon must be soft. Therefore, in computing this process, we use a chiral expansion with Δ-isobar degrees of freedom, the so-called δ-expansion [15], and simultaneously the soft-photon expansion with respect to (w.r.t.) the energy of the emitted photon. The soft-photon expansion is performed to the next-next-to-leading order (NNLO), since this is the order at which the MDM first appears. The chiral expansion is performed to next-to-leading order (NLO). In this way the present work can be viewed as an extension of our recent NLO calculation of pion photoproduction [16,17] to the softly radiative pion photoproduction in the Δ-resonance region.

*vlad@ect.it
†marcvdh@jlab.org

This paper is organized as follows. In Sec. II, we define the electromagnetic moments of the $\Delta(1232)$ and parametrize the $\gamma\Delta\Delta$ vertex. In Sec. III, we recall the relevant chiral Lagrangians and explain the power counting in the δ-expansion scheme, based on which the leading- and next-to-leading-order contributions are then selected. The chiral-loop contributions to both the Δ self-energy and the $\gamma\Delta\Delta$-vertex are evaluated in Sec. IV. In particular, we discuss how the Δ MDM acquires an imaginary (absorptive) part due to the opening of the $\Delta \to \pi N$ decay channel. After discussing the different observables for the $\gamma N \to \pi N\gamma'$ reaction in Sec. V, we present results for these observables within the χEFT framework in Sec. VI. We investigate in detail the sensitivity of different observables on the Δ^+ MDM, and discuss opportunities for experiment. Section VII summarizes the main points and conclusions of the paper.

II. ELECTROMAGNETIC MOMENTS OF THE Δ

Consider the coupling of a photon to a Δ, Fig. 1. The matrix element of the electromagnetic current operator J^μ

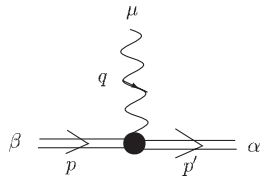

FIG. 1. The $\gamma\Delta\Delta$ vertex. The four-momenta of the initial (final) Δ and of the photon are given by p (p') and q, respectively. The four-vector indices of the initial (final) spin $3/2$ fields are given by β (α), and μ is the four-vector index of the photon field.

between spin $3/2$ states can be decomposed into four multipole transitions: a Coulomb monopole (C0), a magnetic dipole (M1), an electric quadrupole (E2), and a magnetic octupole (M3). We first write its Lorentz-covariant decomposition which exhibits manifest electromagnetic gauge invariance:

$$\begin{aligned}\langle\Delta(p')|eJ^\mu(0)|\Delta(p)\rangle &\equiv \bar{u}_\alpha(p')\Gamma^{\alpha\beta\mu}_{\gamma\Delta\Delta}(p',p)u_\beta(p)\\ &= -e\bar{u}_\alpha(p')\Big\{e_\Delta F_1^*(Q^2)g^{\alpha\beta}\gamma^\mu + \frac{i}{2M_\Delta}\Big[F_2^*(Q^2)g^{\alpha\beta} + F_4^*(Q^2)\frac{q^\alpha q^\beta}{(2M_\Delta)^2}\Big]\sigma^{\mu\nu}q_\nu\\ &\quad + \frac{F_3^*(Q^2)}{(2M_\Delta)^2}\Big[q^\alpha q^\beta\gamma^\mu - \frac{1}{2}q\cdot\gamma(g^{\alpha\mu}q^\beta + g^{\beta\mu}q^\alpha)\Big]\Big\}u_\beta(p),\end{aligned} \tag{2}$$

where F_i^* are the $\gamma^*\Delta\Delta$ form factors, $Q^2 \equiv -q^2 \geq 0$ is the photon virtuality with $q \equiv p' - p$, e_Δ is the electric charge in units of e (e.g., $e_{\Delta^+} = +1$), such that $F_1^*(0) = 1$, u_α represents the spin-$3/2$ Δ vector spinor. The relation to the multipole decomposition [18,19] can be written in terms of the magnetic dipole (μ_Δ), electric quadrupole (Q_Δ), and magnetic octupole (O_Δ) moments, given by

$$\mu_\Delta = \frac{e}{2M_\Delta}[e_\Delta + F_2^*(0)], \tag{3a}$$

$$Q_\Delta = \frac{e}{M_\Delta^2}\Big[e_\Delta - \frac{1}{2}F_3^*(0)\Big], \tag{3b}$$

$$O_\Delta = \frac{e}{2M_\Delta^3}\Big[e_\Delta + F_2^*(0) - \frac{1}{2}(F_3^*(0) + F_4^*(0))\Big]. \tag{3c}$$

III. EFFECTIVE LAGRANGIAN AND POWER COUNTING

The construction of the SU(2) chiral Lagrangian with the pion, nucleon, and Δ-isobar degrees of freedom has recently been reviewed [20,21]. Here we only specify the terms relevant to the NLO calculation of the $\gamma N \to \pi N\gamma'$ process. The Lagrangian is organized in orders of the pion momentum and mass: $\mathcal{L} = \sum_i \mathcal{L}^{(i)}$, with i indicating the order. In terms of the photon (A_μ), pion (π^a), nucleon (N), and Δ-isobar (Δ_μ) fields, we have

$$\begin{aligned}\mathcal{L}^{(1)} &= \bar{N}\Big(i\not{D} - M_N + \frac{g_A}{2f_\pi}\tau^a\not{D}\pi^a\gamma_5\Big)N\\ &\quad + \bar{\Delta}_\mu(i\gamma^{\mu\nu\alpha}D_\alpha - M_\Delta\gamma^{\mu\nu})\Delta_\nu\\ &\quad + \frac{h_A}{2f_\pi M_\Delta}[i\bar{N}T^a\gamma^{\mu\nu\lambda}(D_\mu\Delta_\nu)D_\lambda\pi^a + \text{H.c.}],\\ \mathcal{L}^{(2)} &= \frac{1}{2}D_\mu\pi^a D^\mu\pi^a - \frac{1}{2}m_\pi^2\pi^2\\ &\quad + \frac{3eg_M}{2M_N(M_N+M_\Delta)}[i\bar{N}T^3\partial_\mu\Delta_\nu\tilde{F}^{\mu\nu} + \text{H.c.}]\\ &\quad + \frac{ie}{2M_\Delta}\bar{\Delta}_\mu\frac{1}{2}[1 + \kappa_\Delta^{(S)} + 3(1+\kappa_\Delta^{(V)})\mathcal{T}_3]\Delta_\nu F^{\mu\nu},\\ \mathcal{L}^{(3)} &= \frac{-3eg_E}{2M_N(M_N+M_\Delta)}\bar{N}T^3\gamma_5(\partial_\mu\Delta_\nu)F^{\mu\nu} + \text{H.c.},\end{aligned} \tag{4}$$

where $F^{\mu\nu}$ and $\tilde{F}^{\mu\nu}$ are the electromagnetic field strength and its dual; D_μ is the electromagnetic covariant derivative defined for the various fields as follows:

$$\begin{aligned} D_\mu \pi^a &= \partial_\mu \pi^a + e\varepsilon^{ab3} A_\mu \pi^b \\ D_\mu N &= \partial_\mu N - ie\tfrac{1}{2}(1+\tau^3) A_\mu N \\ D_\mu \Delta_\nu &= \partial_\mu \Delta_\nu - ie\tfrac{1}{2}(1+3\mathcal{T}^3) A_\mu \Delta_\nu. \end{aligned} \tag{5}$$

The antisymmetrized products of γ-matrices are given by $\gamma^{\mu\nu} = \frac{1}{2}[\gamma^\mu, \gamma^\nu]$, $\gamma^{\mu\nu\alpha} = i\varepsilon^{\mu\nu\alpha\beta}\gamma_\beta\gamma_5$, etc. The explicit form of the isospin matrices T^a and $\mathcal{T}^a$ has been specified in our previous paper [17].

There are 8 dimensionless low-energy constants appearing in Eq. (4): g_A, h_A, g_M, g_E, $\kappa_N^{(S)}$, $\kappa_N^{(V)}$, $\kappa_\Delta^{(S)}$, and $\kappa_\Delta^{(V)}$. To the considered order we may neglect the difference between their values in the chiral limit and at the physical pion mass. The physical values of all but the last two constants are fairly well known: $g_A \simeq 1.267$ is the axial coupling of the nucleon; $h_A \simeq 2.85$ is the $\pi N\Delta$ coupling determined from the πN scattering $P33$ phase-shift [20]; g_M and g_E characterize the electromagnetic $M1$ and $E2$ $N \to \Delta$ transition and are fixed from our fit of the pion-photoproduction observables [17]: $g_M = 2.97$, $g_E = -1$; the isoscalar and isovector anomalous magnetic moments of the nucleon are very well established: $\kappa_N^{(S)} = 0.12$, $\kappa_N^{(V)} = 3.7$.

The determination of $\kappa_\Delta^{(S)}$ and $\kappa_\Delta^{(V)}$—the anomalous magnetic moments of the Δ—is precisely the aim of this work. These low-energy constants will appear as the only free parameters in our calculations, which will then be confronted with either the experimental or lattice QCD data.

The thus introduced anomalous magnetic moments are defined as the deviation from the gyromagnetic ratio ($g = \mu/s$) from 2, the natural value for an elementary particle of any spin s [22–24]. In this notation the magnetic moment of the Δ corresponds with[1]

$$\mu_\Delta = \frac{e}{2M_\Delta}\left(3e_\Delta + \frac{1}{2}\kappa_\Delta^{(S)} + \frac{3}{2}\kappa_\Delta^{(V)}\mathcal{T}_3\right), \tag{6}$$

where $e_\Delta = (1+3\mathcal{T}_3)/2$ is the charge of the Δ in units of e. Note that this definition of the anomalous magnetic moment of the Δ has been recently introduced in [20] and is not widely used. Usually one defines it as a deviation of the magnetic moment from the magneton value: $ee_\Delta/(2M_\Delta)$. Namely, in Eq. (3a), $F_2^*(0)$ corresponds precisely with the conventional definition of the anomalous magnetic moment. The relation between the two conventions is obvious: $\kappa_\Delta^{(S,V)} = F_2^{*(S,V)}(0) - 2$.

A first guideline as to the value of μ_Δ is given by the $1/N_c$ (with N_c the number of colors) expansion of QCD proposed by 't Hooft [25] and Witten [26]. In the large-N_c limit, the baryon sector has an exact contracted SU($2N_f$) symmetry, where N_f is the number of light quark flavors. For three light quark flavors, this results in the approximate SU(6) spin-flavor symmetry of QCD, which underlies many quark model results. In this limit the nucleon and Δ are degenerate, and their magnetic moments satisfy: $\mu_\Delta = e_\Delta \mu_p$, where $\mu_p \simeq 2.793\mu_N$ is the magnetic moment of the proton. Note that this relation yields a qualitatively different result for the gyromagnetic ratio of nucleon and Δ: while $g_p \simeq 5.6$ is more than twice the natural value for an elementary particle (i.e., $g = 2$), $g_\Delta \simeq 2.5$ is very close to the natural value.

A. Expansion about the resonance

The chiral power counting in the presence of the Δ-isobar field is also thoroughly discussed in the literature (see Refs. [20,21] for reviews). Here we adopt the "δ counting" scheme [15], where the Δ-resonance excitation energy,

$$\Delta \equiv M_\Delta - M_N \simeq 0.3 \text{ GeV}, \tag{7}$$

is treated differently from the pion mass. One thus has an expansion with two distinct light scales: m_π and Δ. For power-counting purposes, one assumes the following relation between the two:

$$\frac{m_\pi}{\Lambda} \sim \left(\frac{\Delta}{\Lambda}\right)^2, \tag{8}$$

where $\Lambda \sim 1$ GeV stands for the scale of chiral symmetry breaking, $4\pi f_\pi$, as well as other heavy scales, such as the nucleon mass. The power 2 in Eq. (8) is chosen because it is the closest integer power for the relation between these parameters in nature.

The power counting is then done in orders of $\delta = \Delta/\Lambda$, and the power-counting index of a given graph depends on whether the generic momentum p is in the *low-energy region*: $p \sim m_\pi \sim \delta^2$; or in the *resonance region*: $p \sim \Delta \sim \delta$. Such an energy-dependent power counting turns out to be important for a correct size estimate of the *one-Delta-reducible* (ODR) graphs, which contain Δ-isobar propagators of the type

$$S_{\text{ODR}} = \frac{1}{p - \Delta}. \tag{9}$$

In the vicinity of the resonance these propagators diverge, unless a whole class of ODR graphs is resummed, leading to a "dressed" ODR propagator:

$$S^*_{\text{ODR}} = \frac{1}{p - \Delta - \Sigma}, \tag{10}$$

where Σ is the self-energy. The expansion for the Δ-isobar self-energy begins with p^3 and hence is of order δ^3 in the resonance region. Therefore, for

$$|p - \Delta| \leq \delta^3, \tag{11}$$

[1]It is understood that the magnetic moment of a resonance is a complex quantity (see the discussion of the imaginary part of the Δ MDM in the following section). Nonetheless, where not explicitly specified we denote by μ_Δ the real part of the Δ MDM.

the ODR propagators count as δ^{-3}. The condition Eq. (11) can be considered as a stricter definition of the resonance region.

B. Low-energy expansion

The radiative pion-photoproduction experiments designed to measure the Δ-resonance magnetic dipole moment are done near the resonance energy with the observation of a low-energy photon in the final state. This means the energy of the initial photon ω is in the resonance region, $\omega \sim \delta$, while the energy of the final photon, ω', is soft. The expansion in ω' can thus be done akin the usual low-energy expansion (LEX), i.e., the full amplitude is expanded as

$$f(\omega, \omega') = \frac{f_{-1}(\omega)}{\omega'} + f_0(\omega) + f_1(\omega)\omega' + \cdots = \sum_{i=-1} f_i \omega'^i. \tag{12}$$

The dependence of f_i's on ω, m_π and Δ can then be computed according to the δ-counting:

$$f_i = \sum_n f_i^{(n)} \delta^n, \qquad \text{with } \delta \simeq \{\omega/\Lambda, \Delta/\Lambda, (m_\pi/\Lambda)^{1/2}\}. \tag{13}$$

It is not difficult to see that the Δ's MDM starts to enter at order ω'. Therefore, we shall need to have a complete calculation of all three terms written out in Eq. (12) in order to perform a model-independent extraction of the MDM.

As far as the expansion in δ is concerned, we shall restrict ourselves to NLO. We therefore begin with the pion photoproduction at NLO, given by the graphs in Fig. 2, where the blob on the Δ propagator and the $\gamma N\Delta$ vertex indicate that those are corrected by the chiral loops as shown in Fig. 3. For the Born terms, only the electric coupling of the photon with energy ω contributes to NLO. Note also that to this order, only the imaginary part of the

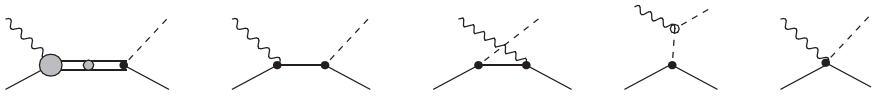

FIG. 2. Diagrams for the $\gamma N \to \pi N$ reaction at NLO in the δ-expansion, considered in this work. Double lines represent the Δ propagators.

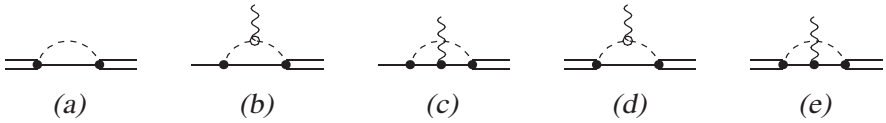

FIG. 3. Chiral-loop corrections considered in this work. Double lines represent the Δ propagators.

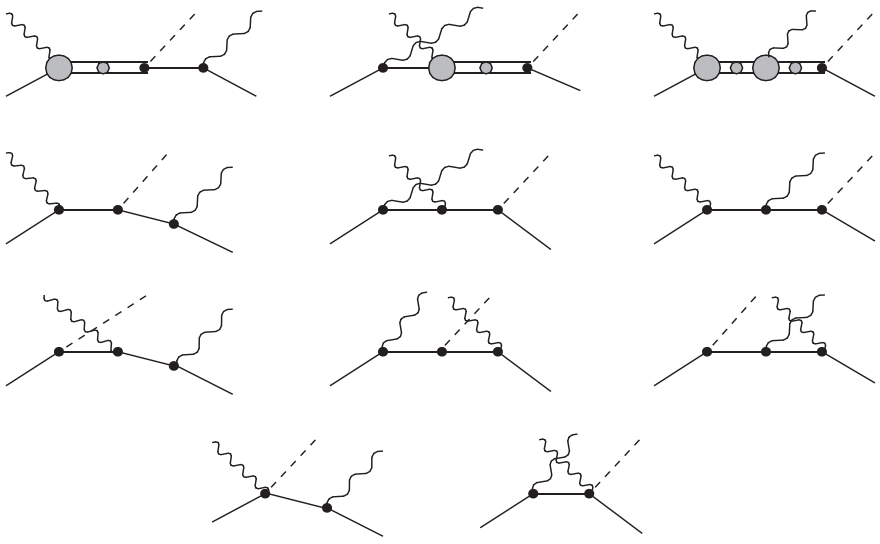

FIG. 4. Diagrams for the $\gamma p \to \pi^0 p\gamma'$ reaction at NLO in the δ-expansion, considered in this work. Double lines represent the Δ propagators. For the $\gamma p \to \pi^+ n\gamma'$ reaction, the pion-pole diagrams where either of the two photons couples to the charged pion are taken into account.

loop corrections contributes, while the effect of the real parts is limited to the renormalization of the appropriate masses and coupling constants. This is why the analogous graphs with the $\pi\Delta$ loops are omitted—they do not produce imaginary contributions in the Δ-resonance region.

The minimal insertion of the final photon in the NLO photoproduction amplitude yields the radiative pion-photoproduction graphs in Fig. 4, where the blob on the $\gamma\Delta\Delta$ vertex indicates the inclusion of the chiral corrections in Figs. 3(d) and 3(e). The graphs in Fig. 4 provide a complete NLO description of the f_i amplitudes in Eq. (12), provided the Δ MDM contribution from $\mathcal{L}^{(2)}$ is included in the $\gamma\Delta\Delta$ vertex.

To summarize, the graphs in Fig. 4, with chiral corrections (Fig. 3), represent a complete calculation of the radiative pion-photoproduction amplitude to NNLO in ω' and NLO in the δ-expansion.

IV. CHIRAL LOOPS

The chiral-loop corrections considered in this work are comprised of the Δ self-energy [Fig. 3(a)], $\gamma N\Delta$-vertex [Figs. 3(b) and 3(c)], and $\gamma\Delta\Delta$-vertex [Figs. 3(d) and 3(e)] corrections. To present the result of our calculations we introduce the following dimensionless quantities:

$$\alpha_p = (p^2 + M_N^2 - m_\pi^2)/2p^2, \tag{14a}$$

$$\beta_p = (p^2 - M_N^2 + m_\pi^2)/2p^2, \tag{14b}$$

which have the interpretation of an energy fraction carried by, respectively, the nucleon and the pion in the loop (hence, $\alpha + \beta = 1$). Furthermore, the corresponding 3-momentum fraction is given by

$$\lambda_p = \frac{1}{2p^2}\sqrt{p^2 - (M_N + m_\pi)^2}\sqrt{p^2 - (M_N - m_\pi)^2} = \sqrt{\alpha_p^2 - \frac{M_N^2}{p^2}} = \sqrt{\beta_p^2 - \frac{m_\pi^2}{p^2}}. \tag{15}$$

A. Self-energy

The result for the Δ self-energy can be written as

$$\Sigma_\Delta^{\alpha\beta}(p) = \frac{\not{p}}{p^2}\gamma^{\alpha\beta\sigma}p_\sigma\Sigma_\Delta(\not{p}), \tag{16}$$

where $\Sigma_\Delta(\not{p})$ has the Lorentz form of a spin-1/2 self-energy, in this case is given by

$$\Sigma_\Delta(\not{p}) = \left(\frac{h_A}{8\pi f_\pi}\right)^2\frac{p^4}{M_\Delta^2}\int_{-\alpha_p}^{1-\alpha_p} dx(\alpha_p\not{p} + M_N)(x^2 - \lambda_p^2) \times [l_p + \ln(x^2 - \lambda_p^2 - i\varepsilon)], \tag{17}$$

where $l_p = -2/(4-d) + \gamma_E - 1 - \ln(4\pi\Lambda^2/p^2)$, with $d \simeq 4$ the number of dimensions, $\gamma_E \simeq 0.5772$ the Euler constant, and Λ the renormalization scale in dimensional regularization.

Note that on the mass shell one simply has

$$\bar{u}_\alpha(p)\Sigma_\Delta^{\alpha\beta}(p)u_\beta(p) = -\bar{u}_\alpha(p)\Sigma_\Delta(\not{p})u^\alpha(p) = \Sigma(M_\Delta), \tag{18}$$

where u_α is the vector spinor of the free Δ solution of the following equations: $(\not{p} - M_\Delta)u_\alpha(p) = 0 = p^\alpha u_\alpha(p) = \gamma^\alpha u_\alpha(p)$, $\bar{u}_\alpha u^\alpha = -1$.

We use the on-mass-shell renormalization, such that M_Δ is the physical mass and the field renormalization constant satisfies $\mathrm{Re}Z_\Delta = 1$. This amounts to introducing a counterterm which subtracts the first two terms in the expansion of the self-energy around the physical mass,

$$\Sigma_\Delta(\not{p}) = \Sigma_\Delta(M_\Delta) + \Sigma'_\Delta(M_\Delta)(\not{p} - M_\Delta) + \cdots. \tag{19}$$

We subtract the real parts only. Subtracting the imaginary part of the self-energy would violate unitarity.

Working at NLO in the EFT expansion, we neglect completely the self-energy contributions beyond the orders written explicitly in Eq. (19). Thus, the only contributions that survive the renormalization and expansion are the following:

$$\mathrm{Im}\Sigma_\Delta(M_\Delta) = \frac{\pi}{2}M_\Delta C^2\int_{-\lambda}^{\lambda} dx(\alpha + r)(x^2 - \lambda^2) = -(2\pi/3)M_\Delta C^2(\alpha + r)\lambda^3, \tag{20a}$$

$$\mathrm{Im}\Sigma'_\Delta(M_\Delta) = \frac{\pi}{2}C^2\int_{-\lambda}^{\lambda} dx(x + \alpha) \times [x^2 - \lambda^2 - 2(\beta - x)(x + \alpha + r)] = -2\pi C^2\lambda\left[\alpha\beta(\alpha + r) - \frac{1}{3}\lambda^2(r + r^2 - \mu^2)\right], \tag{20b}$$

where $C = M_\Delta h_A/(8\pi f_\pi)$, $\alpha = \alpha(M_\Delta^2)$, $\beta = \beta(M_\Delta^2)$, $\lambda = \lambda(M_\Delta^2)$. The first term in the expansion has the usual interpretation in terms of the width: $\mathrm{Im}\Sigma_\Delta = -\Gamma_\Delta/2$. Using the empirical value of $\Gamma_\Delta^{(\mathrm{exp})} \simeq 115$ MeV, we deduce the value of $h_A \simeq 2.85$.

The resulting Δ propagator can then be written as

$$S(p)^{\mu\nu} = \frac{1}{Z_\Delta}\frac{1}{(\gamma\cdot p - \bar{M}_\Delta)}\left\{-g^{\mu\nu} + \frac{1}{3}\gamma^\mu\gamma^\nu + \frac{1}{3\bar{M}_\Delta}(\gamma^\mu p^\nu - \gamma^\nu p^\mu) + \frac{2}{3\bar{M}_\Delta^2}p^\mu p^\nu\right\}, \tag{21}$$

where the wave function renormalization constant Z_Δ and complex mass $\bar{M}_\Delta$ are given by

$$Z_\Delta = 1 - i\,\mathrm{Im}\Sigma'_\Delta(M_\Delta), \tag{22}$$

$$\bar{M}_\Delta = M_\Delta - i\Gamma_\Delta/2Z_\Delta. \tag{23}$$

B. The absorptive MDM

Considering the chiral-loop corrections to the $\gamma\Delta\Delta$-vertex [see Fig. 3(d) and 3(e)], we shall focus on

the imaginary parts only. As mentioned above, the real parts can be renormalized away to the considered order. Certainly this is possible only when we work in the vicinity of the resonance and for the physical pion masses. The behavior of the Δ MDM away from the physical pion mass will be discussed in a forthcoming publication.

It is convenient to write the general Lorentz structure of the chiral correction to the electromagnetic current of the Δ in the following form:

$$\langle \Delta' | J^\mu | \Delta \rangle = -e \bar{u}_\alpha(p') \Big[\gamma^\mu F(q^2) + \frac{(p'+p)^\mu}{2M_\Delta} G(q^2) \Big] u^\alpha(p), \tag{24}$$

where $q = p' - p$ is the photon momentum, u^α is the Rarita-Schwinger vector spinor, F and G are electromagnetic form factors. We have omitted the electric quadrupole and magnetic octupole terms here because they enter at higher order in the LEX, Eq. (12). In this notation, the correction to the MDM is given by $eF(0)/2M_\Delta$. In what follows we limit ourselves to the case of real photons, $q^2 = 0$.

The contribution of the graphs [Figs. 3(d) and 3(e)] to the absorptive part of the electromagnetic form factors can be written, respectively, as [7]

$$\begin{aligned} \mathrm{Im}F^{(d)} &= -\pi C^2 \int_{-\lambda}^{\lambda} dx (x+\alpha) \\ &\quad \times \Big[\frac{1}{2}(x^2-\lambda^2) - (x+\alpha)(x+\alpha+r) \Big] \\ &= 2\pi C^2 \lambda [\alpha^3 + r(\alpha^2+\lambda^2) + 2\lambda^2 \alpha], \end{aligned} \tag{25a}$$

$$\mathrm{Im}G^{(d)} = \pi C^2 \int_{-\lambda}^{\lambda} dx (x+\alpha)(\mu^2 - r^2 - 2x)(x+\alpha+r), \tag{25b}$$

$$\begin{aligned} \mathrm{Im}F^{(e)} &= -\pi C^2 \int_{-\lambda}^{\lambda} dx (x+\beta) \\ &\quad \times \Big[x^2 - \lambda^2 - \frac{1}{2}(1+\beta+x+r)^2 + 2(x+\beta)^2 \Big] \\ &= -(4\pi/3) C^2 \lambda [(\alpha - 2\beta + 4r)\lambda^2 + 3\alpha\beta^2 + 3r\mu^2], \end{aligned} \tag{25c}$$

$$\mathrm{Im}G^{(e)} = -2\pi C^2 \int_{-\lambda}^{\lambda} dx (x+\beta)^2 (\alpha - x + r), \tag{25d}$$

where $r = M_N/M_\Delta$, $\mu = m_\pi/M_\Delta$, whereas C, α, β, and λ are defined below Eq. (20).

The electromagnetic gauge symmetry imposes an intricate relation among a linear combination of these functions and the self-energy. Namely, writing the Ward-Takahashi identity for each of the charge states of the Δ, we obtain

$$\begin{aligned} &\Delta^{++}\!: F^{(d)} + G^{(d)} + F^{(e)} + G^{(e)} = -2\Sigma'_\Delta, \\ &\Delta^{+}\!: \tfrac{1}{3}(F^{(d)} + G^{(d)}) + \tfrac{2}{3}(F^{(e)} + G^{(e)}) = -\Sigma'_\Delta, \\ &\Delta^{0}\!: -\tfrac{1}{3}(F^{(d)} + G^{(d)}) + \tfrac{1}{3}(F^{(e)} + G^{(e)}) = 0, \\ &\Delta^{-}\!: -(F^{(d)} + G^{(d)}) = \Sigma'_\Delta, \end{aligned} \tag{26}$$

where

$$\Sigma'_\Delta = \partial / \partial \not{p} \, \Sigma_\Delta(\not{p})|_{\not{p} = M_\Delta} \tag{27}$$

is the first derivative of the Δ self-energy. In deriving these relations we have assumed that the vertex correction and the self-energy are computed to the same order and are renormalized in the same scheme. Since for now we are interested only in the absorptive parts, we shall not be addressing here the details of renormalization.

Using the empirical values for the couplings and masses (e.g., $C \simeq 1.51$), we find

$$\begin{aligned} &\mathrm{Im}F^{(d)} \simeq 2.63, \quad \mathrm{Im}G^{(d)} \simeq -1.98, \quad \mathrm{Im}F^{(e)} \simeq 1.11, \\ &\mathrm{Im}G^{(e)} \simeq -0.45, \quad \mathrm{Im}\Sigma'_\Delta \simeq -0.655, \end{aligned} \tag{28}$$

and hence can verify the relations [Eq. (26)] numerically. The absorptive part of the Δ-resonance MDM is then found to be [in units of $(e/2M_\Delta)$]

$$\begin{aligned} \mathrm{Im}\mu_{\Delta^{++}} &= \mathrm{Im}[F^{(d)} + F^{(e)}] \simeq 3.74, \\ \mathrm{Im}\mu_{\Delta^{+}} &= \tfrac{1}{3}\mathrm{Im}[F^{(d)} + 2F^{(e)}] \simeq 1.62, \\ \mathrm{Im}\mu_{\Delta^{0}} &= \tfrac{1}{3}\mathrm{Im}[-F^{(d)} + 2F^{(e)}] \simeq -0.14, \\ \mathrm{Im}\mu_{\Delta^{-}} &= -\mathrm{Im}F^{(d)} \simeq -2.63. \end{aligned} \tag{29}$$

We checked our result in two independent ways: first, by calculating the loop integrals as outlined above, and second by directly calculating the corresponding phase space integrals, using Cutkosky rules. We checked analytically that both calculations give the same result for the imaginary part of the different Δ MDMs.

In the heavy-baryon limit (M_N, $M_\Delta \to \infty$), we find

$$\mathrm{Im}F^{(d)} \to \frac{h_A^2 M_\Delta}{16\pi f_\pi^2} \sqrt{\Delta^2 - m_\pi^2}, \tag{30a}$$

$$\mathrm{Im}F^{(e)} \to 0, \tag{30b}$$

and thus for the Δ^+ MDM, for example, we obtain

$$\mathrm{Im}\,\mu_{\Delta^+} = \frac{h_A^2 M_\Delta}{48\pi f_\pi^2} \sqrt{\Delta^2 - m_\pi^2} (e/2M_\Delta). \tag{31}$$

In this limit we can directly compare the present result to the results of an analogous EFT calculation of Hacker *et al.* [27]. We find that our results differ by a factor of 2, for any charge states of the Δ. For example, for the Δ^+, Ref. [27] has $\mathrm{Im}\mu_{\Delta^+} = g^2 M_\Delta/(24\pi f_\pi^2)\sqrt{\Delta^2 - m_\pi^2}(e/2M_\Delta)$, where $g = h_A/2$ is the $\pi N \Delta$ coupling used in that work. In addition, the numerical discrepancy between our results is further increased due to smaller values of the Δ mass and

width ($M_\Delta \simeq 1210$ MeV, $\Gamma_\Delta \simeq 100$ MeV) used in Ref. [27].

We conclude this section with a word on the interpretation of the absorptive MDMs. They apparently quantify the change in the width of the resonance that occurs in an external magnetic field B:

$$\Delta\Gamma = 2\,\mathrm{Im}\mu_\Delta \vec{B}\cdot\vec{n}_s, \tag{32}$$

where $\vec{n}_s$ is the direction of the resonance's spin; see Ref. [28] for more details. Equivalently, one may look for a change in the lifetime of the resonance:

$$\Delta\tau/\tau = -2\,\mathrm{Im}\mu_\Delta \vec{B}\cdot\vec{n}_s\tau, \tag{33}$$

where $\tau = 1/\Gamma$ is the lifetime. Such a change in the lifetime appears to be extremely small in moderate magnetic fields and is difficult to be observed directly. On the other hand, there is perhaps a possibility to compute the absorptive MDMs of hadron resonances in lattice QCD where the effect of arbitrarily large magnetic fields on the width can in principle be studied.

Also, in a reaction such as the radiative pion photoproduction, there are sensitivities on the absorptive part of the Δ MDM, which in the future could lead to its independent determination from experiment. Until then, we are compelled to use the χEFT predictions [Eq. (29)] in our subsequent analysis of this reaction.

V. OBSERVABLES FOR THE $\gamma N \to \pi N\gamma'$ REACTION

To access the MDM of the Δ^+, we consider the radiative pion photoproduction process on a nucleon, i.e., the $\gamma N \to \pi N\gamma'$ reaction. In this section we define a few useful observables of this reaction.

In the discussion of observables it is customary to denote the incoming photon energy by E_γ (instead of ω as above) and the outgoing photon energy by E'_γ (instead of ω'). In the rest of the paper we shall adhere to this notation. Furthermore, all cross sections will be given in the center-of-mass (c.m.) system of the initial γN state. All kinematical quantities will also be quoted in the c.m. system, except for the incoming photon energy which we traditionally denote by its *lab* system value E_γ^{lab}.

The $\gamma N \to \pi N\gamma'$ reaction cross section $d\sigma/dE'_\gamma d\Omega_\pi d\Omega_\gamma$ is fivefold differential w.r.t. to the outgoing photon energy E'_γ, and w.r.t. the solid angles of outgoing pion and photon. Because measuring a fivefold differential cross section with sufficient precision is very challenging, we shall also consider several partially integrated cross sections. For example, $d\sigma/dE'_\gamma d\Omega_\pi$ denotes the $\gamma N \to \pi N\gamma'$ cross-section differential w.r.t. the outgoing photon energy and the pion solid angle, where one has integrated over all outgoing photon directions.

It has been shown in Ref. [10] that, in the soft-photon limit (i.e., for outgoing photon energies $E'_\gamma \to 0$), the $\gamma N \to \pi N\gamma'$ observables exhibit a low energy theorem. It is therefore useful to introduce the ratio [10]

$$R \equiv \frac{1}{\sigma_\pi} E'_\gamma \frac{d\sigma}{dE'_\gamma}, \tag{34}$$

where $d\sigma/dE'_\gamma$ is the $\gamma N \to \pi N\gamma'$ cross section integrated over the pion and photon angles, and σ_π is the angular integrated cross section for the $\gamma N \to \pi N$ process weighted with the bremsstrahlung factor, as detailed in Ref. [10]. This ratio has the property that the low-energy theorem demands: $R \to 1$, as $E'_\gamma \to 0$ (the soft-photon limit).

Besides the unpolarized cross section, we shall also consider here the linear-photon polarization asymmetry Σ^π, defined as

$$\Sigma^\pi = \frac{(d\sigma_\perp/dE'_\gamma d\Omega_\pi) - (d\sigma_\parallel/dE'_\gamma d\Omega_\pi)}{(d\sigma_\perp/dE'_\gamma d\Omega_\pi) + (d\sigma_\parallel/dE'_\gamma d\Omega_\pi)}, \tag{35}$$

where the superscript π in Σ^π indicates that the plane ($\Phi_\pi = 0°$) is defined by the incoming photon and outgoing pion directions, and where $d\sigma_\perp$ ($d\sigma_\parallel$) are the cross sections for perpendicular (parallel) initial photon polarizations, respectively, w.r.t. the above-defined plane.

Analogously, one can define a linear-photon polarization asymmetry Σ^γ as

$$\Sigma^\gamma = \frac{(d\sigma_\perp/dE'_\gamma d\Omega_\gamma) - (d\sigma_\parallel/dE'_\gamma d\Omega_\gamma)}{(d\sigma_\perp/dE'_\gamma d\Omega_\gamma) + (d\sigma_\parallel/dE'_\gamma d\Omega_\gamma)}, \tag{36}$$

where the superscript γ in Σ^γ indicates that the plane ($\Phi_\gamma = 0°$) is defined by the incoming photon and outgoing photon directions, and where $d\sigma_\perp$ ($d\sigma_\parallel$) are the cross sections for perpendicular (parallel) initial photon polarizations, respectively, w.r.t. the above-defined plane.

For circularly polarized photons, the photon asymmetry vanishes for a two-body reaction due to reflection symmetry with respect to the reaction plane. However, for a three-body final state the circular photon polarization asymmetry is finite and can be obtained from the cross section for circular photon polarization. When defining the plane spanned by the incoming photon and the outgoing pion directions as reference plane (i.e., taking $\Phi_\pi = 0°$), the outgoing photon azimuthal angular dependence can be expanded as

$$d\sigma_{\lambda_\gamma} = d\sigma_0 + \sum_{n=1}[\cos(n\Phi_\gamma)d\sigma_n + \lambda_\gamma \sin(n\Phi_\gamma)d\sigma'_n], \tag{37}$$

where $d\sigma$ is a short-hand notation for the c.m. cross section $d\sigma/dE'_\gamma d\Omega_\pi d\Omega_\gamma$, while $\lambda_\gamma = \pm 1$ denotes the photon helicity. Denoting the cross sections for the two different photon helicities by $d\sigma_\pm$, one obtains the unpolarized cross section as

$$\tfrac{1}{2}(d\sigma_+ + d\sigma_-) = d\sigma_0 + \cos\Phi_\gamma d\sigma_1 + \cos 2\Phi_\gamma d\sigma_2 + \cdots, \tag{38}$$

and the difference in photon helicity cross sections as

$$d\sigma_+ - d\sigma_- = 2[\sin\Phi_\gamma d\sigma_1' + \sin 2\Phi_\gamma d\sigma_2' + \cdots]. \tag{39}$$

One can then define a circular photon polarization asymmetry (integrated over the photon polar angle) as

$$\Sigma^\pi_{\rm circ}(\theta_\pi) \equiv \frac{2}{\pi}\frac{\int_{-1}^{+1} d\cos\theta_\gamma \int_0^{2\pi} d\Phi_\gamma 2\sin\Phi_\gamma (d\sigma_+ - d\sigma_-)}{\int_{-1}^{+1} d\cos\theta_\gamma \int_0^{2\pi} d\Phi_\gamma (d\sigma_+ + d\sigma_-)} = \frac{2}{\pi}\frac{\int_{-1}^{+1} d\cos\theta_\gamma d\sigma_1'}{\int_{-1}^{+1} d\cos\theta_\gamma d\sigma_0}, \tag{40}$$

where the superscript π indicates that the reference plane ($\Phi_\pi = 0°$) is defined by the incoming photon and outgoing pion directions.[2]

Similarly we define the circular photon polarization asymmetry for fixed outgoing photon direction and integrated pion direction:

$$\Sigma^\gamma_{\rm circ}(\theta_\gamma) \equiv \frac{2}{\pi}\frac{\int_{-1}^{+1} d\cos\theta_\pi \int_0^{2\pi} d\Phi_\pi 2\sin\Phi_\pi (d\sigma_+ - d\sigma_-)}{\int_{-1}^{+1} d\cos\theta_\pi \int_0^{2\pi} d\Phi_\pi (d\sigma_+ + d\sigma_-)}, \tag{41}$$

where the superscript γ indicates that the reference plane ($\Phi_\gamma = 0°$) is defined by the incoming photon and outgoing photon directions, while the pion solid angle is being fully integrated over.

VI. RESULTS AND DISCUSSION

We now present the numerical results of our χEFT calculation for the $\gamma N \to \pi N \gamma'$ observables. We begin with Fig. 5 which shows the EFT results for the ratio R of the $\gamma p \to \pi^0 p \gamma'$ differential cross section relative to the $\gamma p \to \pi^0 p$ one as defined in Eq. (34), for the linear-photon polarization asymmetry Σ^π defined in Eq. (35), and for the circular photon polarization asymmetry $\Sigma^\pi_{\rm circ}$ defined in Eq. (40). The dashed curves represent our previous results [7], while the solid lines show the result of the present EFT calculation.

The difference between the two calculations is that in Ref. [7] the outgoing photon energy was counted as $O(\delta^2)$, while presently we use the soft-photon expansion, Eq. (12), which required the inclusion of additional bremsstrahlung diagrams. The present calculation thus includes all graphs

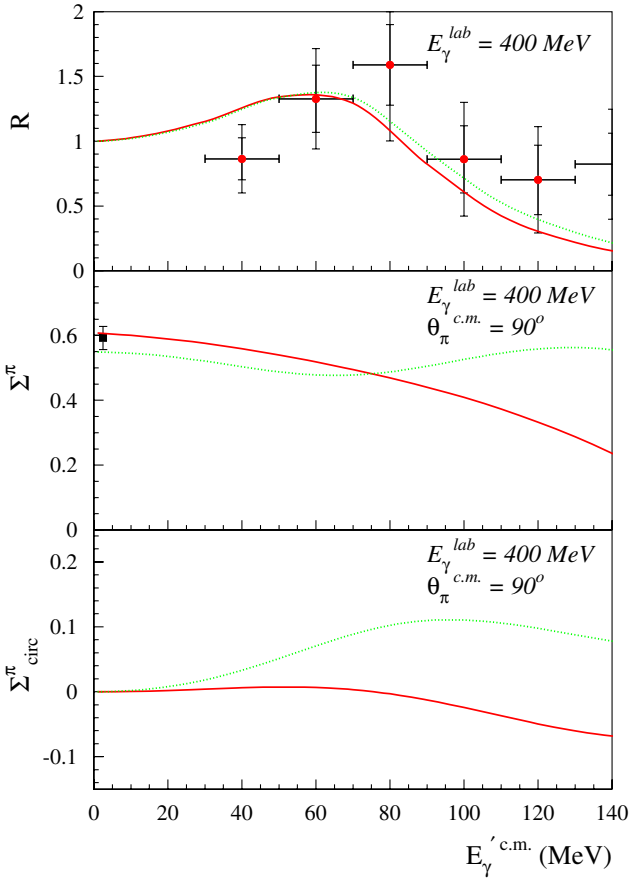

FIG. 5 (color online). Outgoing photon energy dependence for different observables [cross-section ratio R of Eq. (34), linear-photon asymmetry Σ^π, and circular photon asymmetry $\Sigma^\pi_{\rm circ}$] for the resonant EFT calculation of Ref. [7] (green dotted curves) in comparison with the present EFT results (red solid curves), both for Re$\mu_{\Delta^+} = 1$. The data are from Ref. [2], and the linear-photon asymmetry data point for $E'_\gamma = 0$ is $\gamma p \to \pi^0 p$ photon asymmetry from Refs. [29,30].

shown in Figs. 2 and 3, while in the previous calculation nonresonant terms (i.e., graphs without Δ's) were not included. Note that while we now include the nonresonant graphs with the initial photon coupled to the charge of the nucleon or pion, we do not include the coupling of the initial photon to the anomalous magnetic moment of the nucleon (in the nonresonant graphs), as it is suppressed by one more power of δ compared to the electric coupling.

Both calculations in Fig. 5 are shown for $F_2^*(0) = 0$ corresponding with $\mu_{\Delta^+} = 1$ (in Δ magnetons). One sees that the effect of the nonresonant contributions included in the new calculation mainly affects the linear and circular photon asymmetries. For values of E'_γ above about 70 MeV, the nonresonant terms in the present EFT calculation are responsible for the significant decrease in Σ^π in contrast to the previous calculation, where the linear-photon asymmetry is nearly constant over the whole E'_γ range shown in Fig. 5. The effect of the nonresonant terms

[2]The prefactor $2/\pi$ in Eq. (40) arises by defining the asymmetry originally as the ratio of $(d\sigma_+ - d\sigma_-)/(d\sigma_+ + d\sigma_-)$ and integrating the numerator and the denominator over the upper hemisphere only. This is equivalent with the definition of Eq. (40) which involves the $\sin\Phi_\gamma$ moment and where the numerator and the denominator are integrated over the complete photon solid angle.

also shows up in a sizable change in the circular photon asymmetry $\Sigma^{\pi}_{\rm circ}$ with increasing outgoing photon energy.

In the soft-photon limit ($E'_\gamma \to 0$), the present calculation of $\gamma N \to \pi N \gamma'$ goes to the corresponding NLO photoproduction result [17]. The latter has been shown [20] to be in agreement with the well-measured $\gamma p \to \pi^0 p$ observables in a 100 MeV window around the Δ-resonance position. In particular, one sees the nice agreement with the experimental $\gamma p \to \pi^0 p$ linear-photon asymmetry, shown by the data point for Σ^{π} in Fig. 5.

In Fig. 6, we show the outgoing photon energy dependence for the absolute $\gamma p \to \pi^0 p \gamma'$ differential cross sections for different values of μ_{Δ^+}. The cross sections in Fig. 6 have been integrated over all pion and outgoing photon angles and are compared with the first data for this reaction from Ref. [2]. One sees that, at $E_\gamma =$ 350 MeV, all calculations are consistent with the available data. With increasing photon energies (compare $E_\gamma =$ 400 MeV vs 450 MeV in Fig. 6), the present EFT calculation yields an increasing reduction in the absolute cross section relative to the previous calculation. Although this trend is consistent with the existing data, both the precision and sensitivity of these integrated data are insufficient to extract a value of μ_{Δ^+} besides favoring values in the range between 1 and 3Δ magnetons. This is also demonstrated in Fig. 7, where the outgoing photon angular dependence of the cross section is shown when integrated over all pion angles and for all values of $E'_\gamma \geq 30$ MeV. The EFT calculation is consistent with the angular dependence displayed by the first data of Ref. [2], and the higher energy results ($E_\gamma = 450$ MeV) also seem to favor the range $\mu_{\Delta^+} \simeq 1$–3.

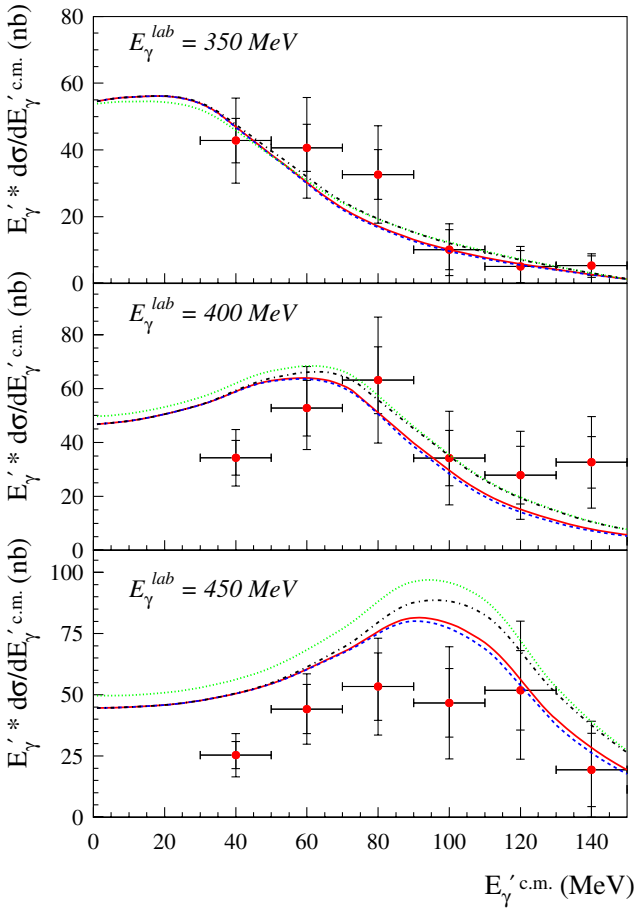

FIG. 6 (color online). Outgoing photon energy dependence of the $\gamma p \to \pi^0 p \gamma'$ cross section fully integrated over outgoing photon and pion angles for three values of the incoming photon energy. The results of the present EFT calculation are shown for three values of μ_{Δ^+}, in units of Δ magnetons: $\mu_{\Delta^+} = 1$ (blue dashed curves), $\mu_{\Delta^+} = 3$ (red solid curves), $\mu_{\Delta^+} = 5$ (black dash-dotted curves). The green dotted curves show the resonant EFT calculation of Ref. [7] for $\mu_{\Delta^+} = 1$. The data are from Ref. [2].

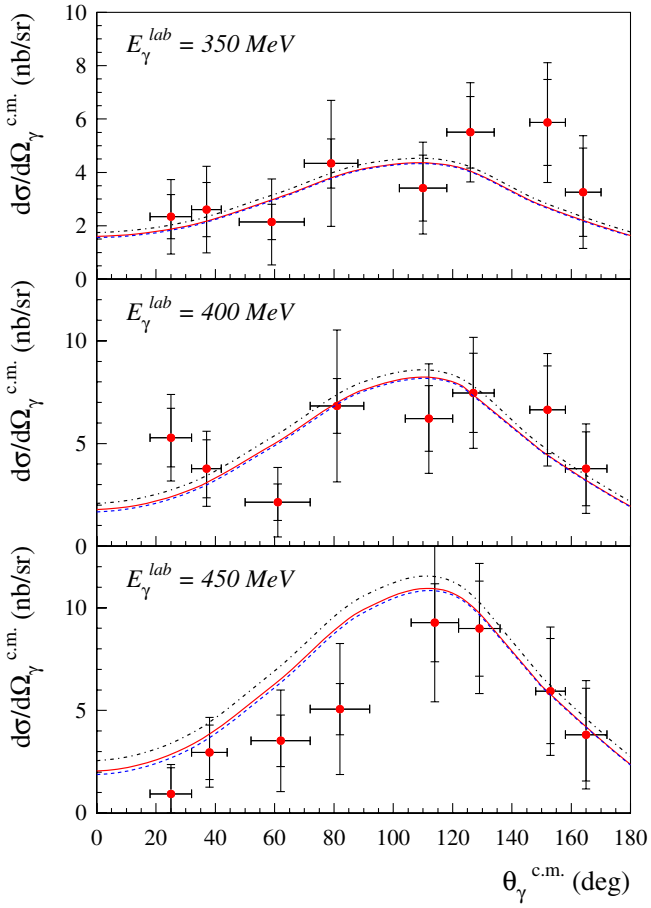

FIG. 7 (color online). Outgoing photon angular dependence of the $\gamma p \to \pi^0 p \gamma'$ c.m. cross section $d\sigma/d\Omega_\gamma$ integrated over outgoing photon energy (for $E'_\gamma \geq 30$ MeV) and pion angles for three values of the incoming photon energy. The results of the present NLO EFT calculation are shown for three values of Reμ_{Δ^+} (in units of Δ magnetons): Re$\mu_{\Delta^+} = 1$ (blue dashed curves), Re$\mu_{\Delta^+} = 3$ (red solid curves), Re$\mu_{\Delta^+} = 5$ (black dash-dotted curves). The data are from Ref. [2].

To enhance the sensitivity to the value of μ_{Δ^+}, we next study $\gamma p \to \pi^0 p \gamma'$ observables that are more differential. In Fig. 8 we show the cross section and linear-photon asymmetry Σ^π, both differential in the outgoing photon energy and pion angle for three values of the outgoing pion angle. One verifies that in the low-energy limit, $E'_\gamma \to 0$, the photon asymmetries of the present EFT calculation are in very good agreement with the photon asymmetry data for the $\gamma p \to \pi^0 p$ reaction as required by the low-energy theorem. With increasing photon energies, the linear-photon asymmetries in the present EFT calculation steadily decrease and show an increasing sensitivity to the value of μ_{Δ^+}, especially around $\theta_\pi^{\text{c.m.}} = 90°$.

The $\gamma p \to \pi^0 p \gamma'$ differential cross sections show a pion angular behavior which can mainly be understood from the following two observations. First, the underlying $\gamma p \to \pi^0 p$ pion angular distribution is peaked at $\theta_\pi^{\text{c.m.}} = 90°$ being approximately symmetrical around this value in the resonance region. Second, the forward-backward asymmetry arises from the bremsstrahlung processes which display a strong enhancement for backward pion angles compared with forward pion angles, as noted in Ref. [10]. One furthermore notices from Fig. 8 that, for photon energies $E'_\gamma \geq 70$ MeV, the unpolarized differential cross sections also show a modest sensitivity to the value of μ_{Δ^+}.

For an increased sensitivity to the Δ^+ MDM, it was suggested in Ref. [10] to measure the asymmetry for a circularly polarized photon beam, as defined in Eqs. (40) and (41). These helicity asymmetries are only nonzero for a three-body final state and vanish in the soft-photon limit $E'_\gamma \to 0$, i.e., when the $\gamma N \to \pi N \gamma'$ process reduces to the two-body, $\gamma N \to \pi N$ process.

In Fig. 9, we show the NLO EFT results for the outgoing photon azimuthal-angle dependence of the $\gamma p \to \pi^0 p \gamma'$ cross sections, for $\Phi_\pi = 0°$ (i.e., the initial photon and outgoing pions define the reference plane). We show both unpolarized cross section (upper panels) and the difference in helicity cross sections for a circularly polarized photon beam.

The azimuthal-angle dependencies of the helicity-averaged and helicity-difference cross sections follow the expansions of Eqs. (38) and (39), respectively. One sees

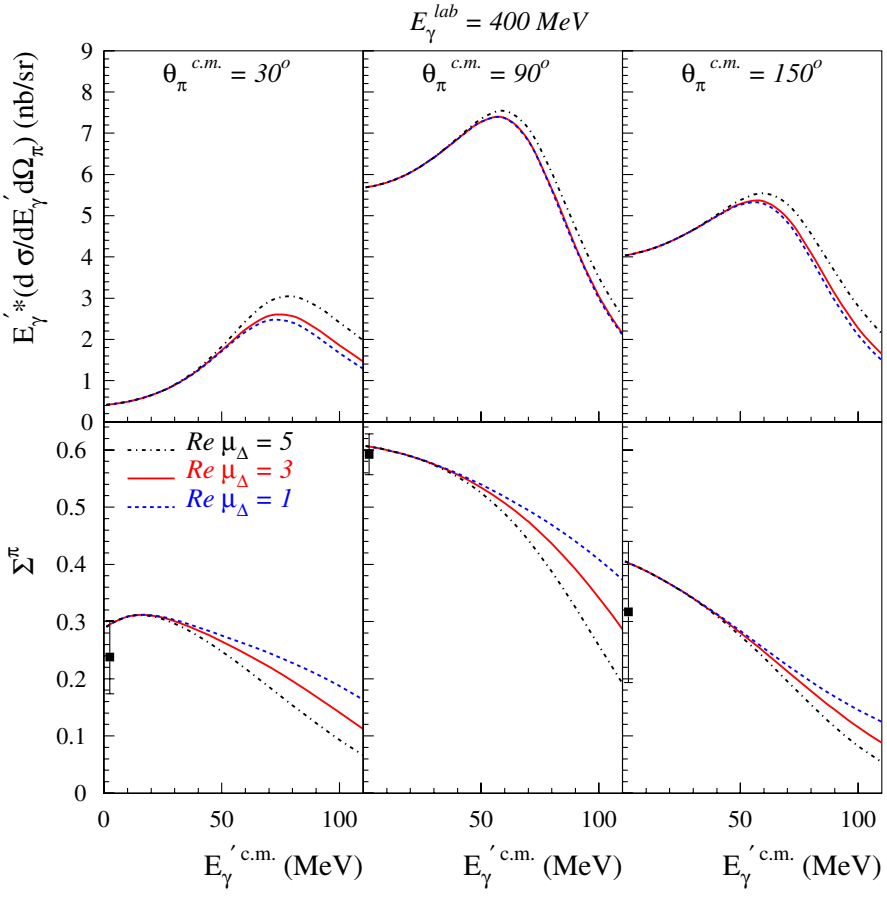

FIG. 8 (color online). Outgoing photon energy dependence of the $\gamma p \to \pi^0 p \gamma'$ cross section (top panels) and linear photon asymmetry (bottom panels) differential with respect to the outgoing photon energy and the pion solid angle for three values of the pion polar angle. The results of the present NLO EFT calculation are shown for three values of $\text{Re}\mu_{\Delta^+}$ (in units of Δ magnetons) as indicated on the figure. The data points for $E'_\gamma = 0$ show the photon asymmetry data of Refs. [29,30] for the $\gamma p \to \pi^0 p$ reaction.

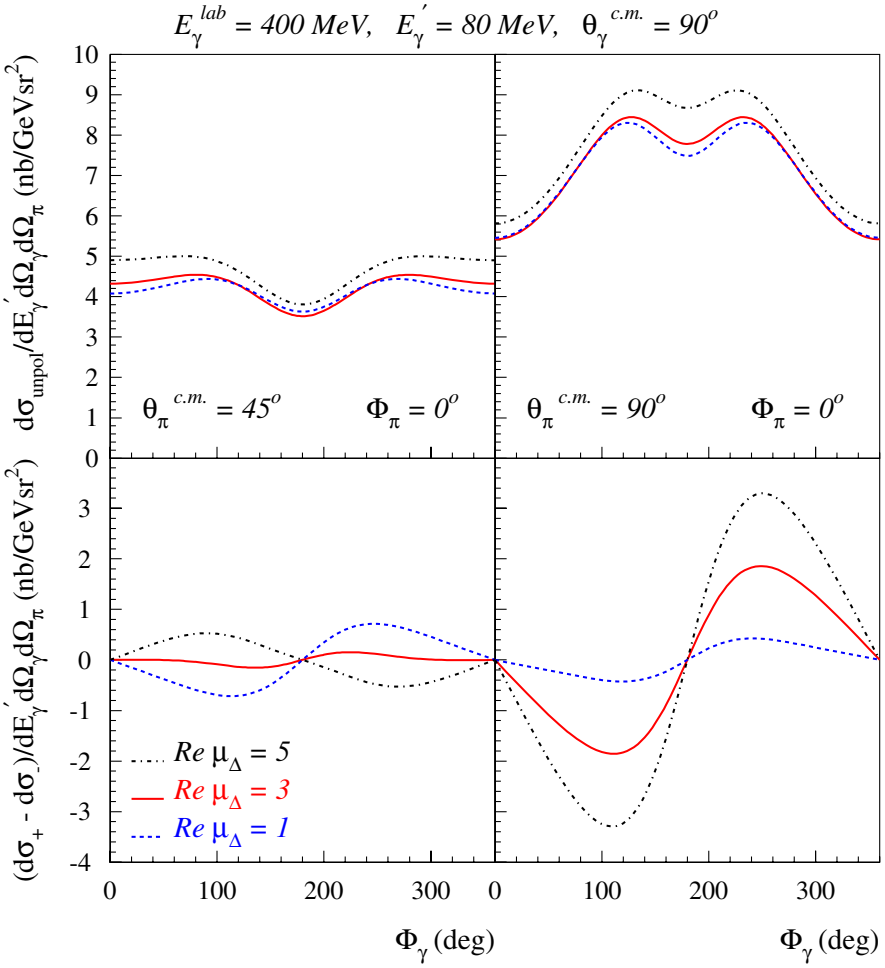

FIG. 9 (color online). Photon azimuthal angular dependence (for $\Phi_\pi = 0°$) of the $\gamma p \to \pi^0 p \gamma'$ fivefold differential cross section for an unpolarized photon beam according to Eq. (38) (top panels), and of the difference in cross sections for a circularly polarized photon beam according to Eq. (39) (lower panels), for two values of the pion polar angle as indicated on the figure. The results of the NLO EFT calculation are shown for three values of $\mathrm{Re}\mu_{\Delta^+}$ (in units of Δ magnetons) as indicated on the figure.

from Fig. 9 that the helicity-difference cross section is dominated by its lowest harmonic, i.e. the term proportional to $\sin\Phi_\gamma$ in Eq. (39). Hence, a measurement of the Φ_γ dependence of the helicity difference cross section allows one to extract its lowest moment, defined as the circular photon polarization asymmetry $\Sigma^\pi_{\mathrm{circ}}$, through Eq. (40).

The EFT predictions for the circular photon polarization asymmetries $\Sigma^\pi_{\mathrm{circ}}$ and $\Sigma^\gamma_{\mathrm{circ}}$ are shown in Figs. 10 and 11, respectively. The NLO EFT calculation first verifies that $\Sigma^\pi_{\mathrm{circ}}$ and $\Sigma^\gamma_{\mathrm{circ}}$ vanish in the limit $E'_\gamma \to 0$. With increasing photon energy, these asymmetries show a very clear sensitivity on the Δ^+ MDM. One sees from Fig. 10 that, for $E_\gamma = 400$ MeV and around $E'_\gamma = 80$ MeV, the asymmetry changes by 0.1 to 0.2 when varying the Δ^+ MDM in the range $\mathrm{Re}\mu_{\Delta^+} = 1$–$5$ of Δ magnetons. Note also that for a given value of $\mathrm{Re}\mu_{\Delta^+}$ both $\Sigma^\pi_{\mathrm{circ}}$ and $\Sigma^\gamma_{\mathrm{circ}}$ change sign between forward and backward angles. The sensitivity of the circular photon polarization asymmetries on $\mathrm{Re}\mu_{\Delta^+}$ can be understood from the observation that these observables arise from the product of the imaginary part of the (resonant) $\gamma p \to \pi^0 p \gamma'$ amplitude with the real part of the $\gamma p \to \pi^0 p \gamma'$ amplitude. Hence, the sensitivity on the real part of the Δ^+ MDM is amplified by multiplication with the large imaginary part, mainly arising from the bremsstrahlung diagrams containing one (resonant) Δ line, where the final photon is radiated from either initial or final proton lines. The photon helicity asymmetry $\Sigma^\pi_{\mathrm{circ}}$ is also sensitive to the imaginary part of the Δ^+ MDM by multiplication with the real part of the $\gamma p \to \pi^0 p \gamma'$ amplitude, as is shown by the dotted curves in Figs. 10 and 11, which have been obtained by switching off the imaginary part of $F_2^*(0)$. Note that in the present EFT calculation the imaginary part of the Δ MDM is obtained as a prediction of the one-loop calculations of Figs. 3(d) and 3(e), as detailed in Sec. IV.

We explore the large sensitivity of $\Sigma^\pi_{\mathrm{circ}}$ on $\mathrm{Re}\mu_{\Delta^+}$ further in Fig. 12. The top panel of Fig. 12 illustrates

that, for a photon beam energy of $E_\gamma = 350$ MeV, where the initial Δ is near resonant, there is a range of about 30–40 MeV in final photon energy where the photon helicity-difference cross section $\sigma_+ - \sigma_-$ is near linear in E'_γ. The bottom panel of Fig. 12 which is obtained from the top panel by dividing through E'_γ shows this slope in E'_γ. One sees that the slope is directly proportional to $\mathrm{Re}\mu_{\Delta^+}$. Although this comes out of the NLO EFT calculation, we like to point out that this is a model-independent feature, resulting from the low-energy theorem for the $\gamma N \to \pi N \gamma'$ process. Indeed in the low-energy expansion of Eq. (12) the dependence on the Δ^+ MDM comes in at the linear term in E'_γ. Because $\Sigma^\pi_{\mathrm{circ}}$ has to vanish (exactly) in the limit $E'_\gamma \to 0$, it starts out with the linear term in the LEX, which also depends linearly on the Δ^+ MDM.

In view of the large sensitivity of $\Sigma^\pi_{\mathrm{circ}}$ on the Δ^+ MDM, it will be of interest to compare with first data for this observable. Such data have recently been taken by the

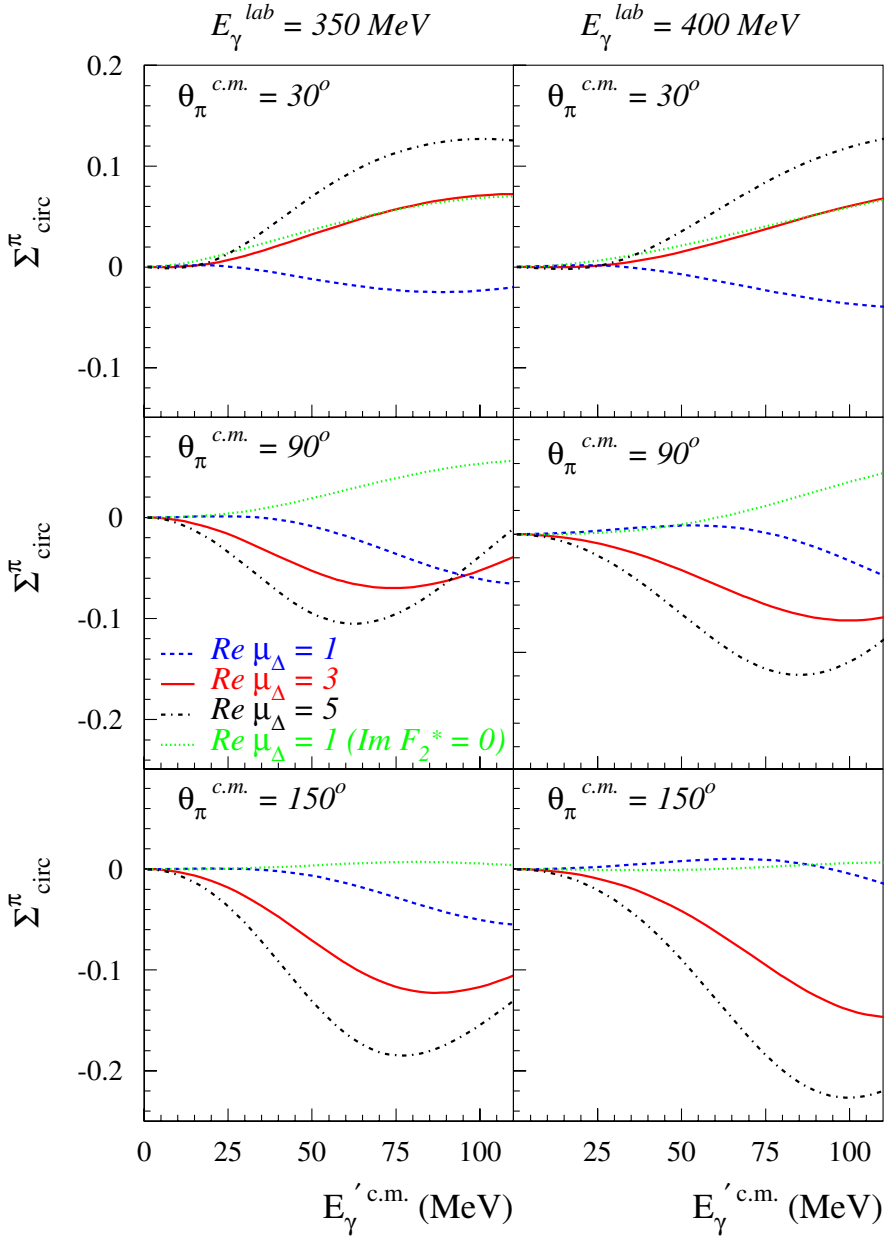

FIG. 10 (color online). Outgoing photon energy dependence of the $\gamma p \to \pi^0 p \gamma'$ circular photon asymmetry differential with respect to the outgoing photon energy and the pion solid angle for three values of the pion polar angle and two incoming photon energies as indicated on the figure. The results of the NLO EFT calculation are shown for three values of $\mathrm{Re}\mu_{\Delta^+}$ (in units of Δ magnetons) as indicated on the figure. The result for $\mathrm{Re}\mu_{\Delta^+} = 1$ is also shown when turning off the imaginary part of F_2^* arising from the $\gamma\Delta\Delta$ vertex corrections, i.e. for $\mathrm{Im}\, F_2^*(0) = 0$ (dotted curves).

Crystal Ball @ MAMI $\gamma p \to \pi^0 p \gamma'$ experiment [6]. Although this experiment was optimized for a linearly polarized photon beam, the experiment also took data with a circularly polarized photon beam. Figure 12 illustrates that a future dedicated measurement of this photon helicity asymmetry for $E'_\gamma \leq 40$ MeV provides an opportunity for a model-independent extraction of the Δ^+ MDM.

Finally, we also show the NLO EFT results for the $\gamma p \to \pi^+ n \gamma'$ reaction in Figs. 13 and 14. By comparing Fig. 8 with Fig. 13, one sees that the ratio of the $\gamma p \to \pi^+ n \gamma'$ to $\gamma p \to \pi^0 p \gamma'$ reactions is around a factor 6, around $\theta_\pi^{\text{c.m.}} = 90°$. The origin of the enhancement in the charged pion channel is the bremsstrahlung from the light charged pion. However, the sensitivity to the resonance properties in the charged pion observables seems to be lesser pronounced than in the neutral pion channel. Nonetheless, the charged pion observables may provide a further test of the present EFT framework in which both channels are calculated simultaneously with the same set of parameters.

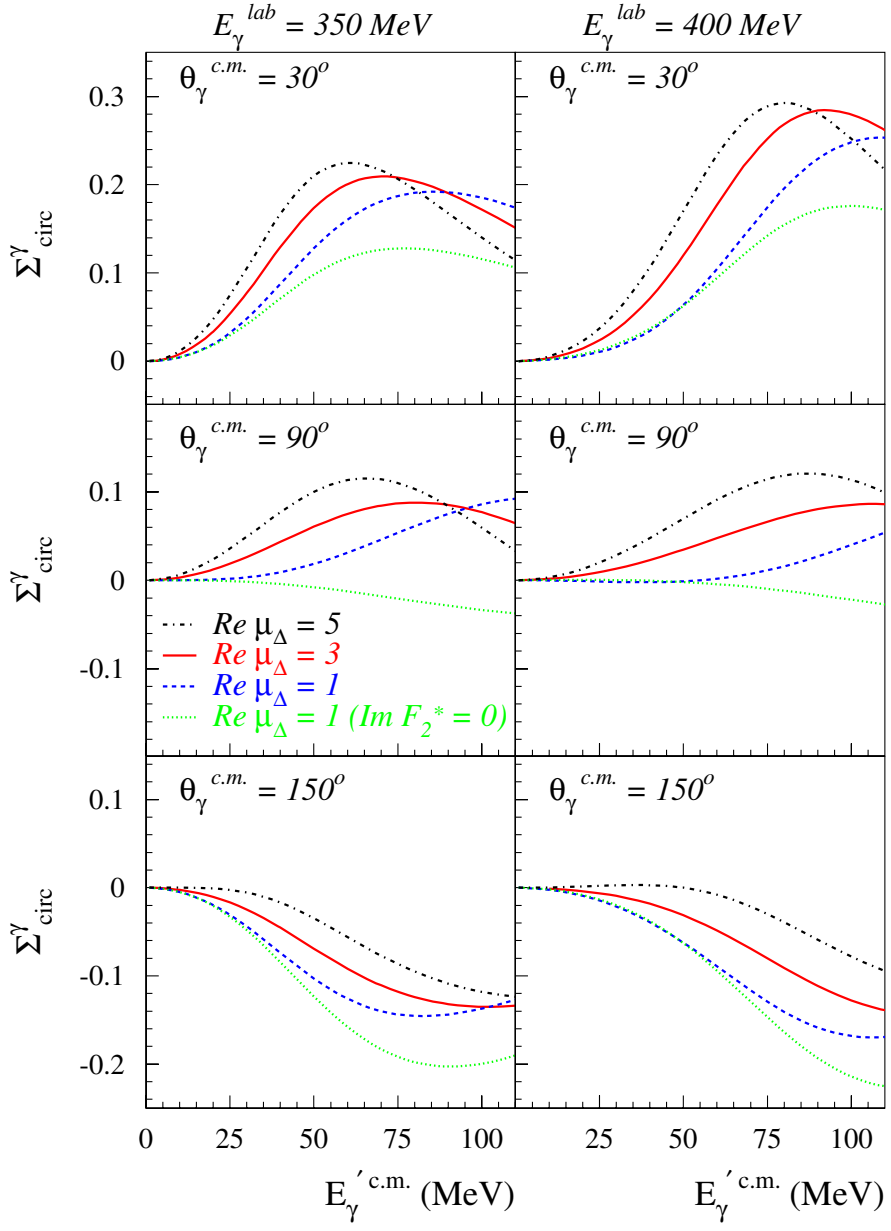

FIG. 11 (color online). Outgoing photon energy dependence of the $\gamma p \to \pi^0 p \gamma'$ circular photon asymmetry differential with respect to the outgoing photon energy and the photon solid angle for three values of the photon polar angle and two incoming photon energies as indicated on the figure. The results of the NLO EFT calculation are shown for three values of $\text{Re}\mu_{\Delta^+}$ (in units of Δ magnetons) as indicated on the figure. The result for $\text{Re}\mu_{\Delta^+} = 1$ is also shown when turning off the imaginary part of F_2^* arising from the $\gamma\Delta\Delta$ vertex corrections, i.e. for $\text{Im}\, F_2^*(0) = 0$ (dotted curves).

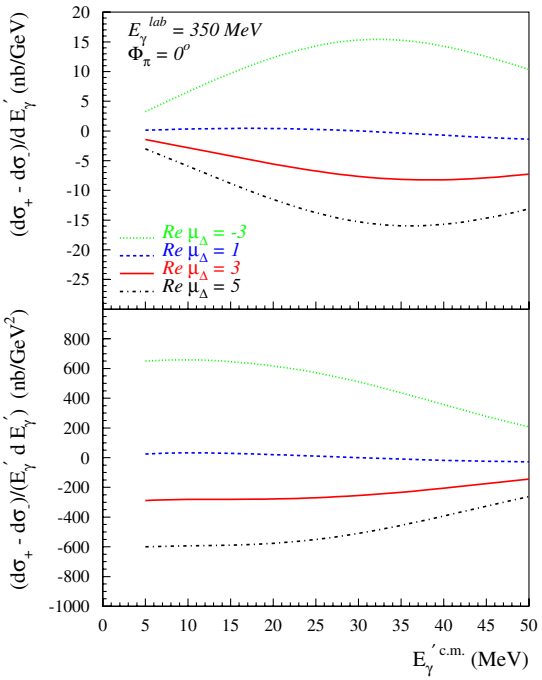

FIG. 12 (color online). Outgoing photon energy dependence of the $\gamma p \to \pi^0 p \gamma'$ photon helicity difference cross sections, differential with respect to the outgoing photon energy, and integrated over the full pion polar angular range (for $\Phi_\pi = 0°$), and over the upper hemisphere for the photon angles. The results of the NLO EFT calculation are shown for four values of Reμ_{Δ^+} (in units of Δ magnetons) as indicated on the figure.

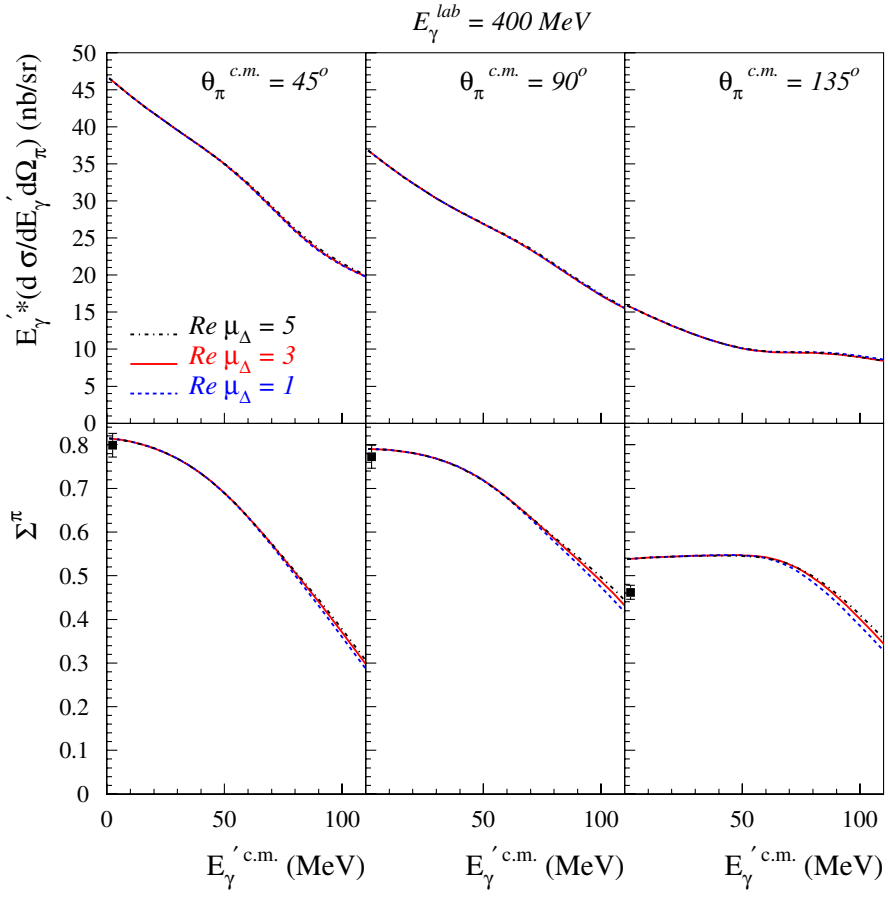

FIG. 13 (color online). Outgoing photon energy dependence of the $\gamma p \to \pi^+ n \gamma'$ cross section (top panels) and linear photon asymmetry (bottom panels) differential with respect to the outgoing photon energy and the pion solid angle for three values of the pion polar angle. The results of the present NLO EFT calculation are shown for three values of Reμ_{Δ^+} (in units of Δ magnetons) as indicated on the figure. The data points for $E'_\gamma = 0$ show the photon asymmetry data of Ref. [29] for the $\gamma p \to \pi^+ n$ reaction.

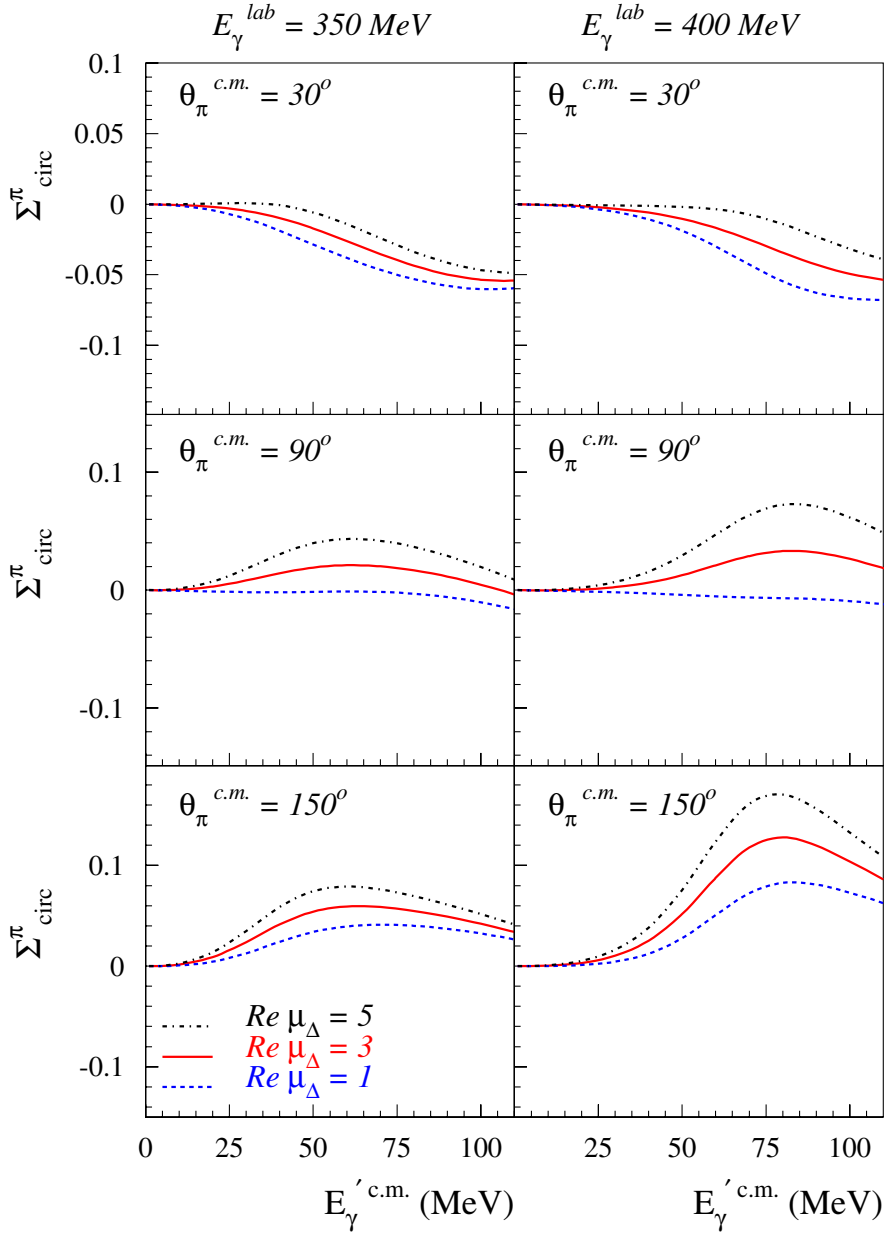

FIG. 14 (color online). Outgoing photon energy dependence of the $\gamma p \to \pi^+ n \gamma'$ circular photon asymmetry differential with respect to the outgoing photon energy and the pion solid angle for three values of the pion polar angle and two incoming photon energies as indicated in the figure. The results of the NLO EFT calculation are shown for three values of $\mathrm{Re}\mu_{\Delta^+}$ (in units of Δ magnetons) as indicated on the figure.

VII. CONCLUSION

In this work we continue to develop and apply a systematic extension of chiral perturbation theory to the Δ-resonance region. Here we have presented the calculation of the imaginary part of the Δ magnetic dipole moment (MDM), as well as a comprehensive study of the observables of the $\gamma N \to \pi N \gamma'$ process in the $\Delta(1232)$-resonance region.

The chiral expansion for the $\gamma N \to \pi N \gamma'$ amplitudes is performed using the so-called δ power-counting scheme, to next-to-leading order (NLO). Furthermore, we use a simultaneous low-energy expansion in the energy ω' of the emitted photon which includes all terms up to $O(\omega')$, where the Δ MDM first appears. To this order, besides the tree-level resonant diagrams, the calculation involves one-loop vertex corrections to the $\gamma N \Delta$ and $\gamma \Delta \Delta$ vertices, as well as nonresonant (Born) diagrams. The only free parameter which enters at this order is the Δ MDM. The one-loop corrections to the $\gamma \Delta \Delta$ vertex give an imaginary (absorptive) part to the Δ MDM, which was quantified.

Concerning the observables, the outgoing photon energy and angular dependencies of the $\gamma p \to \pi^0 p \gamma'$ unpolarized cross section were found to be consistent with first experimental data for this process (assuming about 10% uncertainty of our results, coming from the neglect of higher-order contributions).

We quantified the sensitivities of the $\gamma p \to \pi^0 p \gamma'$ cross section and photon asymmetries to the Δ^+ MDM. It appears that, at low energies of the outgoing photon, the dependence of the cross section and linear-photon asymmetries on the MDM is quadratic, i.e., depends on $|\mu_\Delta|^2$. The asymmetry for a circularly polarized photon beam, however, displays a linear dependence on the Δ^+ MDM. The helicity-difference $\gamma N \to \pi N \gamma'$ cross section for a circularly polarized photon beam vanishes linearly with ω' when approaching the soft-photon limit, its slope being proportional to the Δ^+ MDM. Therefore, a dedicated measurement of the $\gamma p \to \pi^0 p \gamma'$ cross sections with a circularly polarized photon beam provides a unique opportunity for a model-independent extraction of the Δ^+ MDM.

ACKNOWLEDGMENTS

We thank Jambul Gegelia for useful discussions and comments. This work is supported in part by DOE Grant No. DE-FG02-04ER41302 and Contract No. DE-AC05-06OR23177 under which Jefferson Science Associates operates the Jefferson Laboratory. The work of V. P. is partially supported by the European Community-Research Infrastructure Activity under the FP6 "Structuring the European Research Area" program (HadronPhysics, Contract No. RII3-CT-2004-506078).

[1] B. M. K. Nefkens *et al.*, Phys. Rev. D **18**, 3911 (1978); A. Bosshard *et al.*, Phys. Rev. D **44**, 1962 (1991).
[2] M. Kotulla *et al.*, Phys. Rev. Lett. **89**, 272001 (2002).
[3] D. Watts *et al.* (unpublished).
[4] W. M. Yao *et al.* (Particle Data Group), J. Phys. G **33**, 1 (2006).
[5] D. Drechsel and M. Vanderhaeghen, Phys. Rev. C **64**, 065202 (2001).
[6] M. Kotulla (Crystal Ball @ MAMI Collaboration), in Proceedings of the Workshop on the Physics of Excited Nucleons (NSTAR 2007), Bonn, 2007 [Eur. Phys. J. A (to be published)].
[7] V. Pascalutsa and M. Vanderhaeghen, Phys. Rev. Lett. **94**, 102003 (2005).
[8] A. I. Machavariani, A. Faeßler, and A. J. Buchmann, Nucl. Phys. **A646**, 231 (1999); **A686**, 601(E) (2001); A. I. Machavariani and A. Faeßler, arXiv:nucl-th/0703080.
[9] D. Drechsel, M. Vanderhaeghen, M. M. Giannini, and E. Santopinto, Phys. Lett. B **484**, 236 (2000).
[10] W. T. Chiang, M. Vanderhaeghen, S. N. Yang, and D. Drechsel, Phys. Rev. C **71**, 015204 (2005).
[11] V. Bernard, N. Kaiser, and U. G. Meißner, Int. J. Mod. Phys. E **4**, 193 (1995).
[12] G. Ecker, Prog. Part. Nucl. Phys. **35**, 1 (1995).
[13] S. Scherer, Adv. Nucl. Phys. **27**, 277 (2003).
[14] D. B. Kaplan, arXiv:nucl-th/0510023.
[15] V. Pascalutsa and D. R. Phillips, Phys. Rev. C **67**, 055202 (2003).
[16] V. Pascalutsa and M. Vanderhaeghen, Phys. Rev. Lett. **95**, 232001 (2005).
[17] V. Pascalutsa and M. Vanderhaeghen, Phys. Rev. D **73**, 034003 (2006).
[18] H. J. Weber and H. Arenhovel, Phys. Rep. **36**, 277 (1978).
[19] S. Nozawa and D. B. Leinweber, Phys. Rev. D **42**, 3567 (1990).
[20] V. Pascalutsa, M. Vanderhaeghen, and S. N. Yang, Phys. Rep. **437**, 125 (2007).
[21] V. Bernard, Prog. Part. Nucl. Phys. **60**, 82 (2008).
[22] S. Weinberg, in *Lectures on Elementary Particles and Quantum Field Theory*, Brandeis University Summer Institute Vol. 1, edited by S. Deser, M. Grisaru, and H. Pendleton (MIT Press, Cambridge, 1970).
[23] S. Ferrara, M. Porrati, and V. L. Telegdi, Phys. Rev. D **46**, 3529 (1992).
[24] B. R. Holstein, Am. J. Phys. **74**, 1104 (2006).
[25] G. 't Hooft, Nucl. Phys. **B72**, 461 (1974).
[26] E. Witten, Nucl. Phys. **B160**, 57 (1979).
[27] C. Hacker, N. Wies, J. Gegelia, and S. Scherer, Eur. Phys. J. A **28**, 5 (2006).
[28] D. Binosi and V. Pascalutsa, arXiv:0704.0377.
[29] R. Beck *et al.*, Phys. Rev. C **61**, 035204 (2000).
[30] R. Leukel, Ph.D. thesis, University of Mainz, 2001.